Optofluidic particle manipulation in a liquid-core/liquid-cladding waveguide

Kang Soo Lee,[1] Sang Youl Yoon,[1] Kyung Heon Lee,[1] Sang Bok Kim,[1] Hyung Jin Sung,[1,*] and Sang Soo Kim[1,2]

[1]*Department of Mechanical Engineering, KAIST, 291 Daehak-ro, Yuseong-gu, Daejeon 305-701, South Korea*
[2]*sskim@kaist.ac.kr*
[*]*hjsung@kaist.ac.kr*

Abstract: This paper describes a method for particle manipulation in a liquid-core/liquid-cladding optical waveguide system. Step-index and graded-index waveguides were modeled with consideration for, respectively, miscible and immiscible core and cladding fluids. The characteristic motions of four different particles with refractive indices of 1.59, 1.48, 1.37, and 1.22 were examined. The guided beam was assumed to be Gaussian in shape. Our results showed that high-refractive-index particles converged at the center of the core fluid due to a positive gradient force, whereas low-refractive-index particles converged at the flow periphery. The nonlinearity of the particle motion increased as the flow velocity and the guided beam waist decreased and the laser power and the particle size increased. The initial beam waist of the guided beam in the graded-index waveguide did not significantly affect the characteristics of the particle motion due to the effects of diffusion.

OCIS codes: (350.4855) Optical tweezers or optical manipulation; (080.2740) Geometric optical design; (230.7370) Waveguides.

References and links

1. Y. Fainman, L. P. Lee, D. Psaltis, and C. Yang, *Optofluidics: Fundamentals, Devices, and Applications* (McGraw-Hill, 2010).
2. D. V. Vezenov, B. T. Mayers, D. B. Wolfe, and G. M. Whitesides, "Integrated fluorescent light source for optofluidic applications," Appl. Phys. Lett. **86**(4), 041104 (2005).
3. J.-M. Lim, S.-H. Kim, J.-H. Choi, and S.-M. Yang, "Fluorescent liquid-core/air-cladding waveguides towards integrated optofluidic light sources," Lab Chip **8**(9), 1580–1585 (2008).
4. W. Song, A. E. Vasdekis, Z. Li, and D. Psaltis, "Optofluidic evanescent dye laser based on a distributed feedback circular grating," Appl. Phys. Lett. **94**(16), 161110 (2009).
5. W. Song and D. Psaltis, "Pneumatically tunable optofluidic dye laser," Appl. Phys. Lett. **96**(8), 081101 (2010).
6. E. E. Jung, A. J. Chung, and D. Erickson, "Analysis of liquid-to-solid coupling and other performance parameters for microfluidically reconfigurable photonic systems," Opt. Express **18**(11), 10973–10984 (2010).
7. A. L. Vig, R. Marie, E. Jensen, and A. Kristensen, "Optofluidic microscope with 3D spatial resolution," Opt. Express **18**(5), 4158–4169 (2010).
8. I. M. White, S. H. Yazdi, and W. W. Yu, "Optofluidic SERS: synergizing photonics and microfluidics for chemical and biological analysis," Microfluid. Nanofluid. DOI: 10.1007/s10404-012-0962-2 (2012).
9. M. Rosenauer and M. J. Vellekoop, "A versatile liquid-core/liquid-twin-cladding waveguide micro flow cell fabricated by rapid prototyping," Appl. Phys. Lett. **95**(16), 163702 (2009).
10. J. Shi, S. Yazdi, S.-C. S. Lin, X. Ding, I.-K. Chiang, K. Sharp, and T. J. Huang, "Three-dimensional continuous particle focusing in a microfluidic channel *via* standing surface acoustic waves (SSAW)," Lab Chip **11**(14), 2319–2324 (2011).
11. J. Sun, Y. Gao, R. J. Isaacs, K. C. Boelte, P. C. Lin, E. M. Boczko, and D. Li, "Simultaneous on-chip DC dielectrophoretic cell separation and quantitative separation performance characterization," Anal. Chem. **84**(4), 2017–2024 (2012).
12. F. Shen, H. Hwang, Y. K. Hahn, and J.-K. Park, "Label-free cell separation using a tunable magnetophoretic repulsion force," Anal. Chem. **84**(7), 3075–3081 (2012).
13. S. H. Cho, C. H. Chen, F. S. Tsai, J. M. Godin, and Y.-H. Lo, "Human mammalian cell sorting using a highly integrated micro-fabricated fluorescence-activated cell sorter (microFACS)," Lab Chip **10**(12), 1567–1573 (2010).
14. J. P. Beech, S. H. Holm, K. Adolfsson, and J. O. Tegenfeldt, "Sorting cells by size, shape and deformability," Lab Chip **12**(6), 1048–1051 (2012).

#168585 - $15.00 USD Received 15 May 2012; revised 4 Jul 2012; accepted 6 Jul 2012; published 16 Jul 2012

15. A. Ashkin, "Forces of a single-beam gradient laser trap on a dielectric sphere in the ray optics regime," Biophys. J. **61**(2), 569–582 (1992).
16. S. B. Kim, S. Y. Yoon, H. J. Sung, and S. S. Kim, "Cross-type optical particle separation in a microchannel," Anal. Chem. **80**(7), 2628–2630 (2008).
17. Y. Jiang, T. Narushima, and H. Okamoto, "Nonlinear optical effects in trapping nanoparticles with femtosecond pulses," Nat. Photonics **6**, 1005–1009 (2010).
18. C. G. Hebert, A. Terray, and S. J. Hart, "Toward label-free optical fractionation of blood-optical force measurements of blood cells," Anal. Chem. **83**(14), 5666–5672 (2011).
19. T. Kaneta, Y. Ishidzu, N. Mishima, and T. Imasaka, "Theory of optical chromatography," Anal. Chem. **69**(14), 2701–2710 (1997).
20. S. Lin, E. Schonbrun, and K. Crozier, "Optical manipulation with planar silicon microring resonators," Nano Lett. **10**(7), 2408–2411 (2010).
21. A. A. Lall, A. Terray, and S. J. Hart, "On-the-fly cross flow laser guided separation of aerosol particles based on size, refractive index and density-theoretical analysis," Opt. Express **18**(26), 26775–26790 (2010).
22. K. S. Lee, S. Y. Yoon, S. B. Kim, K. H. Lee, H. J. Sung, and S. S. Kim, "Assessment of cross-type optical particle separation system," Microfluid. Nanofluid. **13**(1), 9–17 (2012).
23. R. W. Applegate, Jr., J. Squier, T. Vestad, J. Oakey, and D. W. M. Marr, "Optical trapping, manipulation, and sorting of cells and colloids in microfluidic systems with diode laser bars," Opt. Express **12**(19), 4390–4398 (2004).
24. S.-K. Hoi, Z.-B. Hu, Y. Yan, C.-H. Sow, and A. A. Bettiol, "A microfluidic device with integrated optics for microparticle switching," Appl. Phys. Lett. **97**(18), 183501 (2010).
25. F. Peng, B. Yao, S. Yan, W. Zhao, and M. Lei, "Trapping of low-refractive-index particles with azimuthally polarized beam," J. Opt. Soc. Am. B **26**(12), 2242–2247 (2009).
26. K. T. Gahagan and G. A. Swartzlander, Jr., "Trapping of low-index microparticles in an optical vortex," J. Opt. Soc. Am. B **15**(2), 524–534 (1998).
27. P. A. Prentice, M. P. MacDonald, T. G. Frank, A. Cuschieri, G. C. Spalding, W. Sibbett, P. A. Campbell, and K. Dholakia, "Manipulation and filtration of low index particles with holographic Laguerre-Gaussian optical trap arrays," Opt. Express **12**(4), 593–600 (2004).
28. K. Grujic, O. G. Hellesø, J. P. Hole, and J. S. Wilkinson, "Sorting of polystyrene microspheres using a Y-branched optical waveguide," Opt. Express **13**(1), 1–7 (2005).
29. Y.-F. Chen, X. Serey, R. Sarkar, P. Chen, and D. Erickson, "Controlled photonic manipulation of proteins and other nanomaterials," Nano Lett. **12**(3), 1633–1637 (2012).
30. A. H. J. Yang, S. D. Moore, B. S. Schmidt, M. Klug, M. Lipson, and D. Erickson, "Optical manipulation of nanoparticles and biomolecules in sub-wavelength slot waveguides," Nature **457**(7225), 71–75 (2009).
31. S. Mandal and D. Erickson, "Optofluidic transport in liquid core waveguiding structures," Appl. Phys. Lett. **90**(18), 184103 (2007).
32. H. Schmidt and A. R. Hawkins, "Optofluidic waveguides: I. concepts and implementations," Microfluid. Nanofluid. **4**(1-2), 3–16 (2008).
33. D. B. Wolfe, R. S. Conroy, P. Garstecki, B. T. Mayers, M. A. Fischbach, K. E. Paul, M. Prentiss, and G. M. Whitesides, "Dynamic control of liquid-core/liquid-cladding optical waveguides," Proc. Natl. Acad. Sci. U.S.A. **101**(34), 12434–12438 (2004).
34. K. S. Lee, S. B. Kim, K. H. Lee, H. J. Sung, and S. S. Kim, "Three-dimensional microfluidic liquid-core/liquid-cladding waveguide," Appl. Phys. Lett. **97**(2), 021109 (2010).
35. Y. Yang, A. Q. Liu, L. Lei, L. K. Chin, C. D. Ohl, Q. J. Wang, and H. S. Yoon, "A tunable 3D optofluidic waveguide dye laser *via* two centrifugal Dean flow streams," Lab Chip **11**(18), 3182–3187 (2011).
36. K. S. Lee, S. Y. Yoon, K. H. Lee, S. B. Kim, H. J. Sung, and S. S. Kim, "Radiation forces on a microsphere in an arbitrary refractive index profile," J. Opt. Soc. Am. B **29**(3), 407–414 (2012).
37. R. Bernini, E. De Nuccio, A. Minardo, L. Zeni, and P. M. Sarro, "Liquid-core/liquid-cladding integrated silicon ARROW waveguides," Opt. Commun. **281**(8), 2062–2066 (2008).
38. H. Bruus, *Theoretical Microfluidics* (Oxford University Press, 2008).
39. B. E. A. Saleh and M. C. Teich, *Fundamentals of Photonics* (Wiley, 2007).
40. M. M. Wang, E. Tu, D. E. Raymond, J. M. Yang, H. Zhang, N. Hagen, B. Dees, E. M. Mercer, A. H. Forster, I. Kariv, P. J. Marchand, and W. F. Butler, "Microfluidic sorting of mammalian cells by optical force switching," Nat. Biotechnol. **23**(1), 83–87 (2005).
41. K. H. Lee, S. B. Kim, K. S. Lee, and H. J. Sung, "Enhancement by optical force of separation in pinched flow fractionation," Lab Chip **11**(2), 354–357 (2011).
42. S. B. Kim, H. J. Sung, and S. S. Kim, "Nondimensional analysis of particle behavior during cross-type optical particle separation," Appl. Opt. **48**(22), 4291–4296 (2009).

1. Introduction

Optofluidics, a compound word formed from the words photonics and fluidics, describes the research field in which optical and microfluidic technologies are combined. Optofluidics includes approaches in which the optical properties of a fluid may be changed simply by replacing the working fluid with a fluid having different optical properties [1]. We have obtained an optically smooth interface or gradient across flows formed by two fluid streams

#168585 - $15.00 USD Received 15 May 2012; revised 4 Jul 2012; accepted 6 Jul 2012; published 16 Jul 2012

by tuning the diffusion properties between two flowing streams using immiscible or miscible fluids. The field of optofluidics has produced several technologies, including optofluidic microscopy, optofluidic optical components (*e.g.*, fluidic lenses, prism, gratings, and resonators), optofluidic dye lasers, and optofluidic chemical/bio sensors (*e.g.*, based on total internal reflection fluorescence microscope (TIRFM) or surface-enhanced Raman spectroscopy (SERS)) [2–9].

As the demand for particle and biological particle manipulation in microfluidic channels has expanded to the research fields of micro total analysis system (μ-TAS), life sciences, and drug discovery/screening, a variety of particle manipulation methods based on lab-on-a-chip microfluidic systems, have been developed. Thus far, dielectrophoretic, magnetophoretic, hydrodynamic, surface acoustic wave-driven, and optical particle and biological particle manipulation methods have been reported [10–14]. Among these, optical manipulation is the most widely employed because it is noninvasive and relatively easy to implement compared to other methods. Optical particle manipulation using a laser beam was first demonstrated by Ashkin [15]. Since then, numerous optical particle manipulation methods have been developed [16–22]. Radiation forces, which provide the driving force in optical particle manipulation, are composed of two components: scattering and gradient forces, which act parallel and perpendicular to the direction of the illumination beam, respectively. In general, the scattering force exerts a force on the particles along the direction of the illumination beam if the thermophoretic effects due to absorption of the beam power by the surrounding medium can be neglected. The effects of the gradient force depend on the contrast between the refractive indices of the particle and the surrounding medium. Several researchers have developed optical manipulation systems for high-refractive-index ($n_{\text{particle}} > n_{\text{liquid}}$) or low-refractive-index ($n_{\text{particle}} < n_{\text{liquid}}$) particles, where n_{particle} and n_{liquid} are the refractive indices of the particle and the working fluid, respectively [23–27]. Depending on the system configuration, either the scattering or gradient force could be utilized as the major driving force for particle manipulation. The characteristics of optical particle manipulation were evaluated in terms of the physical and chemical properties of the particles, such as the size, shape, and refractive index. More recently, optofluidic-based particle manipulation systems have been reported [28–31]. Several types of waveguide designs, including slot waveguides and plasmonic waveguides, have been employed to realize these systems.

Waveguides may be divided into two categories: total internal reflection- (TIR-) and interference-based waveguides. Evanescent, liquid-core, nanoporous cladding, liquid-core/liquid-cladding (L^2), and slot waveguides are examples of TIR-based waveguide systems. Bragg fibers, hollow-core photonic crystal fibers, and antiresonant reflecting optical waveguides (ARROW) are examples of interference-based waveguides [32]. The L^2 optical waveguides, first reported by Wolfe *et al*. [33], has been widely studied in the context of potential applications because they are optically flexible and easily constructed using a core fluid and two cladding fluids. The core fluid is horizontally sandwiched between the cladding fluids. The size of the core may be controlled by the flow rates of the cladding fluids, indicating that it is possible to adjust the number of modes guided through the L^2 waveguide *via* the flow rate balance between the core and cladding fluids. Light delivery and evanescent coupling through microfluidic channels or dye lasers using L^2 waveguide systems have been demonstrated [33–35]. The present L^2 waveguide system has not yet been used for optical manipulation of particles. Furthermore, techniques for continuously manipulating particles based on the particle refractive indices have not yet been investigated.

The present study examined optofluidic particle manipulation in a liquid-core/liquid-cladding (L^2) optical waveguide from a theoretical perspective. Particles with refractive indices either higher or lower than the surrounding medium could be separated *via* the negative of the gradient force. The characteristics of the spherical microparticle motion in the step-index and graded-index (GRIN) waveguides were evaluated in terms of the particle refractive index, flow velocity in a microfluidic channel, particle size, laser beam power, and beam waist of the guided laser. A step-index waveguide was simulated based on two immiscible fluids, and a GRIN waveguide was modeled by solving the time-varying one-

#168585 - $15.00 USD Received 15 May 2012; revised 4 Jul 2012; accepted 6 Jul 2012; published 16 Jul 2012

dimensional diffusion equation. Particles with refractive indices of 1.59, 1.48, 1.37, and 1.22 were considered to model the artificial particles commonly used in optical chromatography. Optical losses along the flow direction and at the liquid-liquid interface were neglected. The guided beam was assumed to be Gaussian in shape. The feasibility of using the system described here for real-time continuous particle separation is discussed.

2. Theory

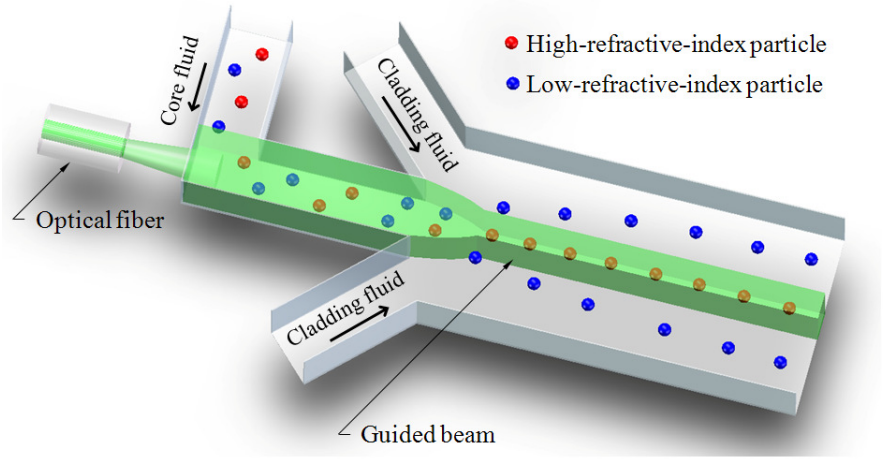

Fig. 1. Schematic diagram of a liquid-core/liquid-cladding (L^2) waveguide particle separation system.

Figure 1 shows a schematic diagram of the liquid-core/liquid-cladding (L^2) waveguide particle separation system. As high- and low-refractive-indices particles flow along the core stream of the L^2 waveguide system, high-refractive-index particles are pulled into the center of the core stream due to the positive gradient force that acts at the highest intensity region of the beam, whereas low-refractive-index particles are repelled from the center of the core due to the negative gradient force, which acts in the opposite direction of the positive gradient force [36].

Figure 2 shows the force balance in the L^2 waveguide particle separation system. The particle motion in the region in which the radiation and hydrodynamic (viscous) forces act can be explained by Newton's second law:

$$\vec{F}_{\text{net}} = m_{\text{p}} \frac{\mathrm{d}\vec{U}}{\mathrm{d}t} = \vec{F}_{\text{rad}} + \vec{F}_{\text{v}}, \tag{1}$$

where $\vec{F}_{\text{net}}$, $\vec{F}_{\text{rad}}$, and $\vec{F}_{\text{v}}$ denote the net force, radiation forces, and viscous drag force on a particle, respectively. m_{p} is the particle mass and $\vec{U}$ is the particle velocity vector. The gravitational force is neglected in Eq. (1). The viscous drag force on a particle is given by

$$F_{\text{v}} = 6\pi\mu r_p U, \tag{2}$$

#168585 - $15.00 USD Received 15 May 2012; revised 4 Jul 2012; accepted 6 Jul 2012; published 16 Jul 2012

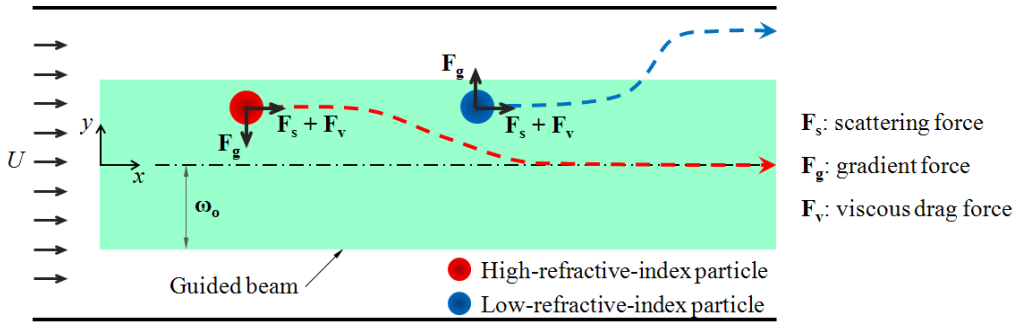

Fig. 2. Force balance in a guided light beam.

where μ is the dynamic viscosity of the working fluid, r_p is the radius of particle and U is the flow velocity. Substitution of Eq. (2) into Newton's second law [Eq. (1)], yields two force equations:

$$m_p \frac{d^2x}{dt^2} = F_s - 6\pi\mu r_p \left(\frac{dx}{dt} - U \right), \tag{3}$$

$$m_p \frac{d^2y}{dt^2} = F_g - 6\pi\mu r_p \frac{dy}{dt}. \tag{4}$$

The flow velocity is assumed to be uniform. F_s and F_g are the scattering and gradient forces, respectively.

The radiation forces, composed of the scattering and gradient forces, can be analytically expressed by either of two different forms: the Rayleigh scattering model and the geometrical optics model [36]. The Rayleigh scattering model is useful for calculating the radiation forces on particles smaller than the wavelength of the illumination beam; however, most optical particle manipulation techniques involve micron-sized particles that are comparable in size to biological cells. Hence, the geometrical optics model, which is useful for calculating the radiation forces on particles larger than the wavelength of the illumination beam, was employed here. In the present study, it was necessary to calculate the radiation forces acting on particles in an arbitrary refractive index profile because the particles experienced nonhomogeneous surrounding media. L^2 waveguide can be constructed to yield an index of refraction profile that is either a step or a gradient function, depending on the characteristics of the core and cladding fluids. Immiscible core and cladding fluids are used to construct step-index waveguides. GRIN waveguides are constructed using miscible core and cladding fluids. Lee *et al*. [36] expressed the scattering and gradient forces on a microsphere embedded in an arbitrary refractive index profile as:

$$\begin{aligned} F_s = \frac{1}{2c} \int_0^{2\pi} \int_0^{\pi/2} I(\rho, x) \Big[n(\rho) \{ 1 + R(\rho) \cos 2\theta_1 \} \\ - n(\rho') T(\rho_k) T(\rho') \cos\alpha \Big] r_p^2 \sin 2\theta_1 d\theta_1 d\varphi, \end{aligned} \tag{5}$$

$$\begin{aligned} F_g = -\frac{1}{2c} \int_0^{2\pi} \int_0^{\pi/2} I(\rho, x) \Big[n(\rho) R(\rho) \sin 2\theta_1 \\ - n(\rho') T(\rho) T(\rho') \sin\alpha \Big] r_p^2 \sin 2\theta_1 \cos\varphi d\theta_1 d\varphi, \end{aligned} \tag{6}$$

#168585 - $15.00 USD Received 15 May 2012; revised 4 Jul 2012; accepted 6 Jul 2012; published 16 Jul 2012

where c denotes the speed of light in free space and $n(\rho)$ and $n(\rho')$ are the refractive indices of the surrounding medium at the first (ρ) and second (ρ') interfaces, respectively [36]. *R* and *T* are the Fresnel reflectance and the Fresnel transmittance, respectively. $I(\rho,x)$ is the beam intensity profile given by:

$$I(\rho,x)=\frac{2P}{\pi\omega(x)^2}\exp\left[-\frac{2\rho^2}{\omega(x)^2}\right], \tag{7}$$

where *P* is the power of the guided beam and $\omega(x)$ is the beam radius along the *x*-direction. The guided beam in the present system has a number of modes. However, the Gaussian assumption is valid because the fundamental mode is prominent compared to other higher-order modes [33,37]

3. Results and discussion

3.1 Refractive index profile

The present study modeled particle motions in the step-index or GRIN waveguides. Each waveguide was simulated by calculating the refractive index profiles for the single core and double cladding streams. The step-index waveguide was modeled as including a certified refractive index matching liquid (*n* = 1.50; Cargille Labs Inc., USA) and de-ionized (DI) water (*n* = 1.33) as the core and cladding liquids, respectively. Since the refractive index liquid is poorly soluble in DI water, the two fluids may produce an excellent step-index waveguide throughout the microfluidic channel. The flow profile in the microfluidic channel minimized mixing, and the core and cladding liquids flowed along the flow direction without interacting. The GRIN waveguide was simulated using an aqueous solution of $CaCl_2$ (8 M, *n* = 1.50) and DI water as the core and cladding liquids, respectively. The diffusion coefficient of $CaCl_2$ was set to $D = 1 \times 10^{-9}$ m^2/s. In general, the refractive index of an aqueous solution is affected by the concentration of the solutes. The relationship between the $CaCl_2$ concentration and the refractive index of the aqueous liquid may be expressed as [33]:

$$n = 1.33547 + \left(0.02192 \times [CaCl_2]\right), \tag{8}$$

where $[CaCl_2]$ denotes the concentration (M) of $CaCl_2$ in an aqueous solution. The refractive index profile in a GRIN waveguide is calculated by solving the time-varying diffusion equation. Diffusion parallel to the direction of flow was neglected. The diffusion equation, governed by Fick's law, is given by [38]:

$$\frac{\partial C}{\partial t} = D\nabla^2 C, \tag{9}$$

where *C* is the concentration of the solute. In the present study, the diffusion equation satisfied the initial conditions

$$C(y,0) = C_o, \qquad -\omega_o \le y \le \omega_o, \tag{10a}$$

$$C(y,0) = 0, \qquad |y| > \omega_o, \tag{10b}$$

and the boundary conditions were

$$C(\pm W/2, t) = 0, \tag{11}$$

where W is the width of the microfluidic channel.

#168585 - $15.00 USD Received 15 May 2012; revised 4 Jul 2012; accepted 6 Jul 2012; published 16 Jul 2012

Figure 3 shows refractive index profiles along the direction of flow in the L^2 waveguide particle separation systems. The width and length of the computational domain over the microfluidic channel were 50 μm and 200 μm, respectively. The width of the core stream at the inlet was 10 μm. The fluid velocity was set to 300 μm/s under the assumption of uniform flow. The step-index waveguide preserved the boundary between the refractive indices of the core and cladding fluids along the flow direction, whereas the refractive index profile of the GRIN waveguide varied continuously along the flow direction due to diffusion of the $CaCl_2$ solute from the core to the cladding fluid. Hence, for the GRIN waveguide, the beam radius shown in Eq. (7) was calculated from the computed refractive index profile for the given *x*-position. Immiscible fluid-fluid interfaces are generally uniform and both hydrodynamically and optically smooth due to the surface tension [1].

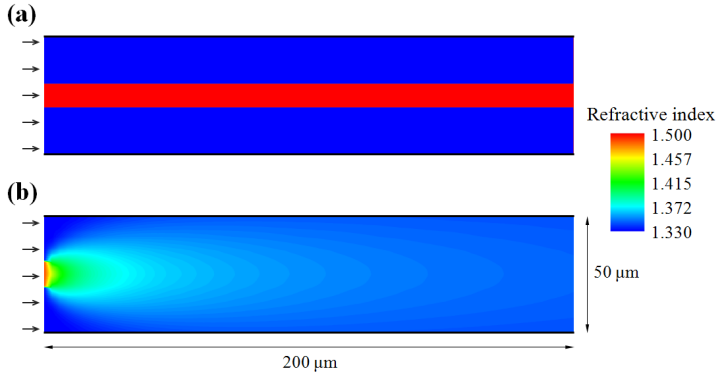

Fig. 3. Refractive index profiles along the direction of flow in the L^2 waveguide particle separation systems: (a) step-index and (b) GRIN waveguides.

3.2 Predicted particle motions with different refractive indices

Microspheres made from polystyrene latex (PSL), poly(methyl methacrylate) (PMMA), silica, and hollow glass, all of which are commonly used in optical manipulation experiments, were modeled as having, respectively, refractive indices of 1.59, 1.48, 1.37, and 1.22.

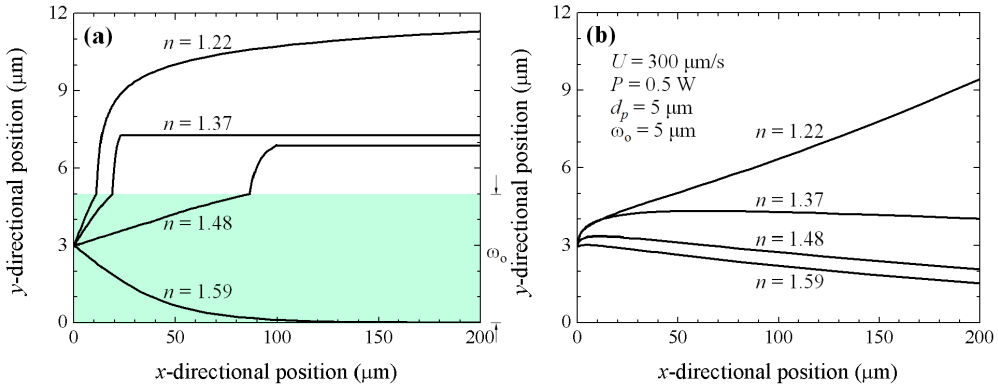

Fig. 4. Trajectories of particles with various refractive indices in the (a) step-index and (b) GRIN waveguides.

Figure 4(a) shows trajectories of particles with various refractive indices in the L^2 step-index waveguide. Particles were injected initially at y = 3 μm. The major driving force for particle separation in this system was the gradient force. Particles with a refractive index of 1.59 were focused at the center of the core stream along the flow direction due to a positive gradient force. Particles with a refractive index of 1.22 diverged from both the core flow and

#168585 - $15.00 USD Received 15 May 2012; revised 4 Jul 2012; accepted 6 Jul 2012; published 16 Jul 2012

the cladding stream along the flow direction due to a negative gradient force. Continuous divergence was observed in both the core and cladding regions for particles with a refractive index exceeding the refractive indices of the core and cladding liquids, leading to a continuous negative gradient force acting on the particle. Particles with refractive indices of 1.48 and 1.37 first diverged from the core and entered the cladding fluids due to a negative gradient force. The particles subsequently flowed parallel to the flow direction at some *y*-position because the refractive indices of these particles were intermediate between the refractive indices of the core and cladding fluids, leading to a balance of forces between the negative and positive gradient forces acting on the fluids. The slope of the particle displacement (*i.e.*, $\mathrm{d}y/\mathrm{d}x$) was higher in the cladding fluid than in the core fluid because the net gradient force acting on a particle increased at the interface between the core and cladding fluids.

Figure 4(b) shows trajectories for particles of various refractive indices in the L^2 GRIN waveguide. The particle motions in the system were less dynamic than in the step-index waveguide system because the beam waist expanded along the flow direction due to solute diffusion from the core fluid to the cladding fluid. This feature of the GRIN waveguide flow may be advantageous in practical applications because the GRIN waveguide can reduce the problems observed in the step-index waveguide, such as modal dispersion. Reduced modal dispersion preserves the shape of the optical intensity profile along the direction of propagation in the guided beam because the differences between the phase speeds of each mode may be reduced [39]. Because the gradient force results from a gradient in the optical force profile, reduced modal dispersion can ensure reliable particle motion. Particles with a refractive index of 1.59 were focused to the center of the core fluid, as was observed in the step-index waveguide. Similarly, particles with a refractive index of 1.22 diverged from the core fluid and flowed with the cladding liquids. Particles with refractive indices of 1.48 and 1.37 first diverged from the core fluid, then slightly converged back toward the core fluid once in the cladding fluids. This behavior resulted from the diffusion of the solute from the core to the cladding fluids. Initially, the particles diverged outward due to the negative gradient force. However, the difference between the refractive indices of the core and cladding liquids lessened along the downstream direction due to diffusion. Hence, the refractive indices of the particles became larger than the refractive index of the surrounding fluid, leading to a positive gradient force.

3.3 Effect of the flow velocity

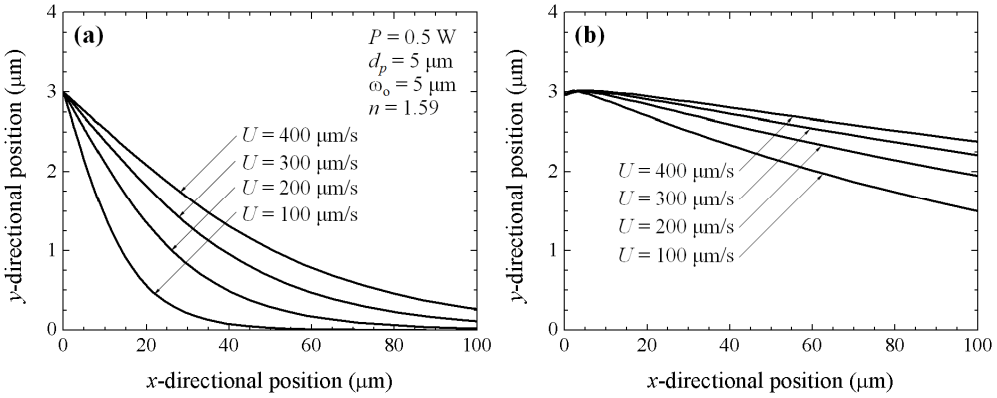

Fig. 5. Trajectories of particles in fluids with a range of velocities in a microfluidic channel: (a) step-index and (b) GRIN waveguides.

The effects of the flow velocity on particle motion in the system were estimated by evaluating the characteristics of the particles in flows with velocities between 100 to 400 μm/s. Figure 5 shows the trajectories of particles flowing with various velocities in the step-index and GRIN

#168585 - $15.00 USD Received 15 May 2012; revised 4 Jul 2012; accepted 6 Jul 2012; published 16 Jul 2012

waveguides. Particles with a refractive index of 1.59 were considered. The force balance diagram shown in Fig. 2 indicates that the force acting perpendicular to the direction to flow (the gradient force) was relatively higher than the force acting parallel to the direction of flow (viscous and scattering forces) for low flow velocities. Hence, the slope of the particle displacement increased as the flow velocity decreased. The slope of the particle displacements was smaller in the GRIN waveguide than in the step-index waveguide, as shown in Fig. 5(b), due to diffusion of the solute from the core to cladding liquids. In the GRIN waveguide, the *y*-directional diffusion increased along a certain distance in the *x*-directional as the flow velocity decreased, leading to a rapid reduction in the refractive index difference between the core and cladding fluids along the direction of flow; however, the higher gradient force due to the low velocity compensated for the decline in the refractive index differences. Therefore, the slope of the particle displacements increased slightly as the flow velocity decreased.

3.4 Effect of the laser power

The presence of a laser beam guided through the waveguide affected the particle motion. This effect was found to be power-dependent, and the effects of laser powers between 0.5 and 2.0 W were examined. Biological particle manipulation techniques (*e.g.*, hydrodynamic, dielectric, electrophoretic, or magnetophoretic) frequently incur unwanted cell damage due to the large amount of energy exerted on the particles. Several studies reported that the optical forces applied within certain laser power ranges did not significantly influence the cell viability measured after application of the optical force [40,41]. Figure 6 shows the trajectories of particles in systems in which laser beams with a range of powers were guided through the L^2 step-index and GRIN waveguide systems. In general, the slope of the particle displacement increased as the laser power increased due to an increase in the gradient force. The particle motions in the optical force field could be explained in terms of the dimensionless number *S* corresponding to the ratio between the optical force and the viscous drag force, as first expressed by Kim et al. [42],

$$S = \frac{\left(nP/\pi c\right)\left(r_p^2/\omega_o^2\right)}{6\pi\mu r_p U}, \tag{12}$$

As *S* increased, the particle motion became nonlinear due to an increase in the optical force. In the step-index waveguide system shown in Fig. 6(a), the slope of the particle displacement became nonlinear as higher laser powers. On the other hand, in the GRIN waveguide system shown in Fig. 6(b) yielded linear particle trajectories in all calculations because the beam waist was extended along the flow direction because solute diffusion from the core to the cladding fluids compensated for the increase in the gradient optical force.

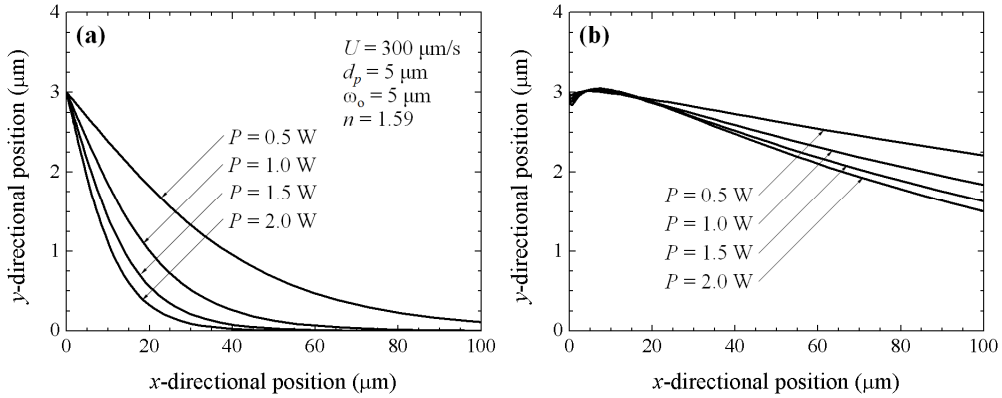

Fig. 6. Trajectories of particles in the L^2 waveguide systems through which were guided laser beams with various powers: (a) step-index and (b) GRIN waveguides.

#168585 - $15.00 USD Received 15 May 2012; revised 4 Jul 2012; accepted 6 Jul 2012; published 16 Jul 2012

3.5 Effects of particle size

The present system provides a model of particle motion in the context of biological particle separation/manipulation for particles with diameters from 1 to 5 μm. Figure 7 shows the particle trajectories for various particle sizes in the L^2 step-index and GRIN waveguide systems. The slope of the particle displacement increased with the particle size in both systems. As the particle size increased, the particle motions became nonlinear due to an increase in the *S* number. This implied that the particles could be separated based on size if the length of the L^2 waveguide were appropriately adjusted. In the GRIN waveguide system, 1 μm particles showed only small displacements. As discussed above, the particle motion could be enhanced by controlling other parameters, such as the laser power and the flow velocity.

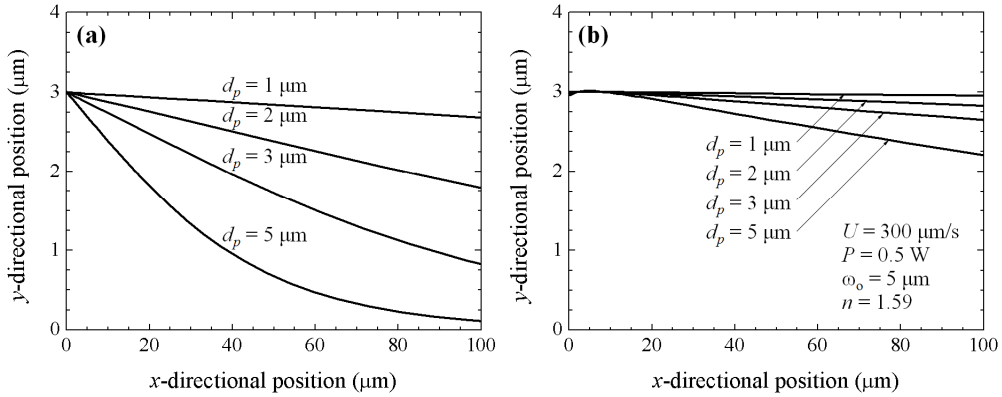

Fig. 7. Particle trajectories for various particle sizes: (a) step-index and (b) GRIN waveguides.

3.6 Effect of the beam waist

Figure 8(a) shows particle trajectories in the presence of beams with a range of initial beam waists in the step-index waveguide system. Because the gradient force was determined by the gradient of the optical intensity, the slope of the particle trajectories increased as the initial beam waist decreased. Simultaneously, particle motions became nonlinear as the beam waist decreased due to a higher *S* number. In the GRIN waveguide shown in Fig. 8(b), however, the initial beam waist did not play an important role in the particle motions because the extension of the beam waist along the flow direction as a result of solute diffusion was so dramatic that the change in the initial beam waist was meaningless.

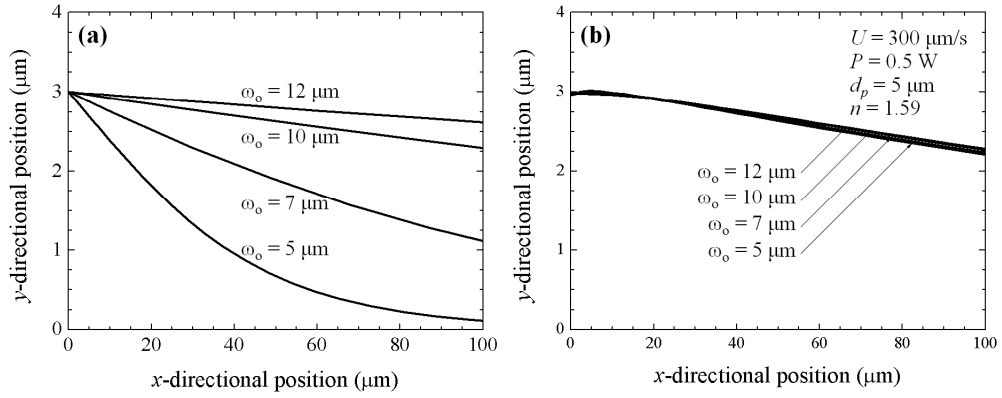

Fig. 8. Trajectories of particles for various initial beam waists: (a) step-index and (b) GRIN waveguides.

#168585 - $15.00 USD Received 15 May 2012; revised 4 Jul 2012; accepted 6 Jul 2012; published 16 Jul 2012

4. Conclusions

In the present study, particle motions in a liquid-core/liquid-cladding waveguide particle separation system were analyzed. The characteristic microparticle motions in both the step-index and graded-index (GRIN) waveguides were evaluated by considering particles with four different refractive indices of 1.59, 1.48, 1.37, and 1.22. The guided beam was assumed to be Gaussian in shape. Our results showed that particles with refractive indices higher than that of the medium (high-refractive-index particles) converged to the center of the core fluid due to a positive gradient force. The opposite behavior was observed for particles with a refractive index lower than that of the medium (low-refractive-index particle). Nonlinearities in the particle motion became more prominent as the flow velocity and beam waist of the guided beam decreased and as the laser power and particle size increased. Interestingly, the initial beam waist of the guided beam did not significantly affect the characteristics of particle motions in the GRIN waveguide system due to solute diffusion. Our results suggest that liquid-core/liquid-cladding waveguides may be useful for applications involving refractive index-driven artificial, functional, or biological particle manipulations. The behavior of the present system may be tuned by controlling the particle size, the laser source power, and the flow velocity, among other parameters.

Acknowledgments

This work was supported by the Creative Research Initiatives (No. 2012-0000246) program of the National Research Foundation of Korea.

#168585 - $15.00 USD Received 15 May 2012; revised 4 Jul 2012; accepted 6 Jul 2012; published 16 Jul 2012